Sodium-Layer Synthetic Beacons for Adaptive Optics

Ronald A. Humphreys, Lee C. Bradley, and Jan Herrmann

■ Using adaptive optics to compensate for atmospherically induced wavefront distortions requires a remote beacon. In astronomical imaging the beacon can be the object of interest or a nearby bright star. For a satellite the beacon can be a retroreflector illuminated by a ground-based laser. Unfortunately, dim stars don't always have bright neighbors, and we cannot place retroreflectors on satellites belonging to unfriendly nations. Synthetic beacons, generated by laser backscatter from the atmosphere, offer a solution to this problem. In 1984 Lincoln Laboratory performed the first measurements on wavefronts propagated through atmospheric turbulence from a synthetic beacon in the mesospheric sodium layer. Lincoln Laboratory has been highly active in the development and evaluation of synthetic beacons since that time. Although military applications initially stimulated the development of synthetic-beacon technology, current interest in synthetic beacons has expanded to include the astronomical community.

Adaptive optics systems for atmospheric-turbulence compensation require information on the wavefront phase distortions introduced by the atmosphere. This information is obtained from a light source or beacon whose wavefront passes through the atmosphere and is measured by the wavefront sensor in the adaptive optics system. In some cases a bright object such as a star provides sufficient light to serve as the beacon. More frequently, however, we must provide the beacon. For example, when the intent is to compensate over the atmospheric path to a satellite, a ground-based laser can illuminate a retroreflector placed on the satellite. Unfortunately, this approach is often inappropriate or impossible; we cannot, after all, expect to place a retroreflector on a satellite belonging to an unfriendly nation. To solve this problem we can use synthetic beacons, which are light sources generated by laser backscatter within the atmosphere. These beacons are produced by using Rayleigh backscatter, or scattering by the air molecules, at altitudes below 20 km, or by using resonant backscatter from the mesospheric sodium layer at an altitude of approximately 90 km (see the box entitled "The Sodium Layer"). This article addresses the use and generation of synthetic beacons in the sodium layer. We also describe the first experiment performed by Lincoln Laboratory to demonstrate the feasibility of using synthetic beacons in the sodium layer.

Particular research interest in the recent past has been in the propagation of ground-based laser beams to uncooperative space targets. Because of the long range (hundreds to thousands of kilometers) and high velocities of these targets, the laser beam must be pointed ahead of the target to hit it, like firing a gun at a moving target. The angle θ between the direction of the target and the direction of the laser beam is known as the *point-ahead angle.* This angle is approximately equal to $2v/c$, where v is the target velocity and c is the velocity of light. For satellites near zenith, the point-ahead angle is typically between 30 and 50 μrad.

At visible and near-infrared wavelengths, the point-ahead angle θ often exceeds the atmospheric-turbulence isoplanatic angle θ_0 by a factor of 5 or more. For simplicity, θ_0 can be regarded as the angle over which

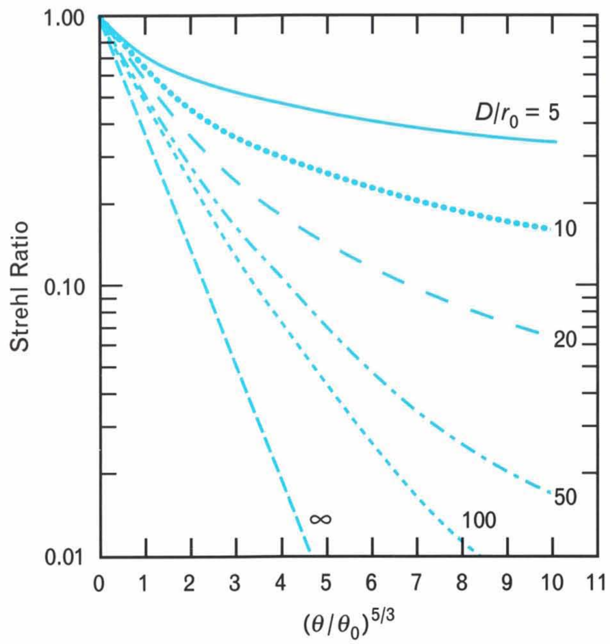

FIGURE 1. The Strehl ratio due to angular (or *point-ahead*) anisoplanatism as a function of $(\theta/\theta_0)^{5/3}$ for several values of D/r_0, as calculated for a commonly used turbulence model. This figure illustrates the reduction in Strehl ratio if the atmosphere is sensed by a beacon placed at an angle θ from the correct location. The angle θ_0 is the isoplanatic angle, D is the receiver aperture diameter, and r_0 is the atmospheric-turbulence coherence length.

the phase distortion of a wavefront propagated through turbulence remains essentially unchanged. Thus the wavefront distortion in the laser-beam direction differs from that in the satellite direction; this effect is known as *angular anisoplanatism.* Figure 1, which is based on calculations made for an atmospheric-turbulence model in common use [1], illustrates the magnitude of this effect on the performance of an optical system. Performance is frequently given in terms of the *Strehl ratio.* This parameter is the ratio of the peak intensity in the far-field spot, or point-source image, of the system to the peak intensity of the spot formed by an equivalent diffraction-limited, or aberration-free, system. Figure 1 shows the Strehl ratio versus $(\theta/\theta_0)^{5/3}$ for values of D/r_0, where D is the receiver aperture diameter and r_0 is the atmospheric-turbulence coherence length (the lateral distance over which a wavefront propagated through turbulence remains coherent). The ratio D/r_0 is a measure of the strength of the turbulence. The figure shows that for values of the point-ahead angle θ larger than θ_0 the system performance is significantly degraded. For these values, even though the satellite may be bright enough to serve as a beacon, it is unsuitable as a beacon for atmospheric-turbulence compensation of the outgoing laser beam. The solution to this problem is to place a synthetic beacon at the point-ahead angle.

Concepts

A synthetic beacon is generated by a ground-based laser that illuminates a column within the atmosphere; backscatter from a part of this column is selected by range gating for use as a synthetic beacon. The backscattered radiation from a synthetic beacon passes through the atmosphere, where it encounters phase distortions resulting from turbulence (and possibly heating of the atmosphere in high-energy laser applications). The distorted wavefront provides an input to the wavefront sensor in the adaptive optics system. Ideally the synthetic beacon should closely resemble a real beacon, i.e., a small, bright source at the proper height and angle to provide accurate information on the wavefront distortions introduced by atmospheric turbulence. In this section we review the general approaches to producing synthetic beacons and the effects of the departure of the synthetic beacon from an ideal source.

The synthetic-beacon concept was apparently conceived independently by several individuals in the early 1980s. Julius Feinleib of Adaptive Optics Associates suggested the use of a laser beam to generate Rayleigh-backscatter synthetic beacons. W. Happer later proposed use of the mesospheric sodium layer [2]. Not until 1985, however, did these concepts reach the open literature [3]. R.Q. Fugate et al. made the first atmospheric-turbulence measurements using Rayleigh-backscatter beacons in 1983 at the U.S. Air Force Weapons Laboratory (now the Phillips Laboratory) [4]. In 1984 Lincoln Laboratory made the first measurements on synthetic beacons in the mesospheric sodium layer [5]. L.A. Thompson and C.S. Gardner have also generated a sodium-layer synthetic beacon [6]. Lincoln Laboratory has been highly active in the development and use of synthetic beacons since its first experiments in 1984.

THE SODIUM LAYER

SEVERAL METALS, probably of meteoritic origin, are present in the upper atmosphere in the form of atoms or ions. The existence of the sodium layer at an altitude of approximately 90 km has been known for at least 60 years. Early measurements of the characteristics of the sodium layer were made by using ground-based spectroscopic instruments to observe the resonance scattering of sunlight from the layer. The presence of the sodium D lines in spectroscopic studies of twilight airglow provided the first evidence of the existence of the layer. (The wavelengths of the sodium D_1 and D_2 lines are 589.6 nm and 589.0 nm, respectively; the D_2 line exhibits the higher level of resonant scattering.)

The difficulty in detecting the spectral lines against the sky background was such that measurements were restricted to twilight conditions for many years. Improvements in the sensitivity of spectrophotometers eventually allowed ground-based measurements to be made in daytime. Daytime measurements of the layer were also made with rocket-borne instruments in the 1960s. With the advent of the tunable dye laser, direct measurements of the characteristics of the layer were made by using laser radar techniques. The first laser radar measurement was reported by M.R. Bowman et al. in 1969 [1], and the technique has remained the favored approach since that time. The laser must be accurately tuned to the wavelength of the selected sodium line, usually the D_2 line at 589 nm, to obtain resonant backscatter from the sodium layer. For efficient operation, the laser should have a spectral bandwidth of 3 GHz or less to provide a good match to the width of the sodium line.

When the need for high-altitude synthetic beacons was recognized in the early 1980s, the sodium layer was readily selected as the primary candidate for this purpose. The atomic resonant transition of sodium lies in the visible spectral region; in addition, the sodium layer has other attractive features for the generation of high-altitude synthetic beacons. The large cross section for resonance scattering (7×10^{-17} m^2-$ster^{-1}$) and the abundance of the sodium atoms result in higher levels of backscatter than for any other species in this altitude region. The abundance refers to the number of atoms projected within a unit cross-sectional area of a vertical column extending over the layer thickness. An average value of the sodium abundance, as measured in our experiments in New Mexico (see main text) is 3×10^{13} atoms-m^{-2}. The abundance of sodium atoms also varies with latitude, time of day, and season; seasonal variations of an order of magnitude have been observed at northern latitudes. Significant increases in abundance have been observed during meteor showers, which supports the theory that meteor ablation replenishes the sodium layer. The thickness of the sodium layer is usually between 10 and 15 km. There appears to be no evidence that holes exist in the sodium layer, although stratification of the layer is occasionally observed.

References

1. M.R. Bowman, A.J. Gibson, and M.C.W. Sandford, "Atmospheric Sodium Measured by a Tuned Laser Radar," *Nature* 221, 456 (1969).

In addition to military applications, synthetic beacons are expected to become a valuable tool for astronomy. When an adaptive optics system is used to improve the performance of ground-based astronomical telescopes, a bright star can serve as a suitable source for turbulence compensation. If the bright star is not the object of interest, it should be within the isoplanatic angle θ_0 of that object to obtain good compensation. The scarcity of bright guide stars for compensation in the visible spectral region has been recognized for several years [7]. A synthetic beacon can be used instead of a bright star, and the astronomical community has recently shown considerable interest in the approach. Further information on the use of synthetic beacons for astronomical applications appears in the article by Ronald R. Parenti in this issue [8].

Figure 2 illustrates a monostatic configuration for the generation and utilization of synthetic beacons. In this configuration the outgoing laser beam and the backscattered photons share the same aperture of an optical system. Note that the laser beam may use only a portion of the aperture, e.g., the area within the central obscuration of a telescope. The beacon laser must be pulsed to allow selection of the beacon altitude and depth by electronically range-gating the backscattered radiation. Without extraordinary measures, the maximum pulse-repetition rate is determined by the length of the pulse and the total transit time through the atmosphere. The limiting pulse-repetition rate varies from approximately 1 kHz for a sodium beacon to many kilohertz for low-altitude beacons. These rates are sufficient for most applications to keep up with changes in the atmospheric turbulence. The monostatic approach can be used to generate both Rayleigh-backscatter and sodium-layer synthetic beacons; researchers at Lincoln Laboratory and other institutions have most commonly used this approach.

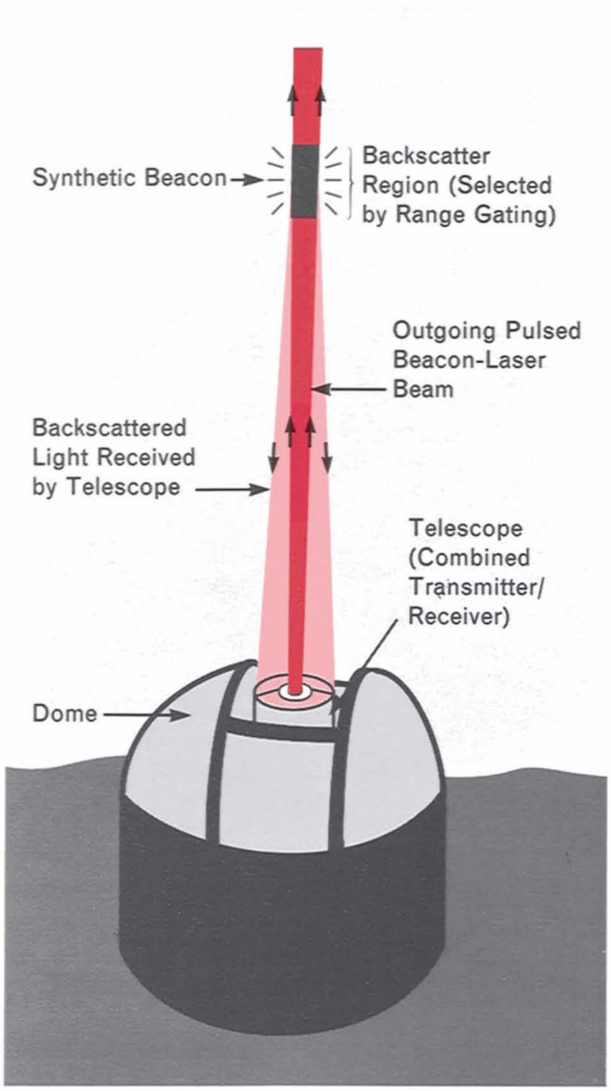

FIGURE 2. The monostatic approach. The beacon-laser beam and the backscattered photons from the synthetic beacon share the same optical-system aperture. Researchers at Lincoln Laboratory and other institutions have commonly used this approach.

Figure 3 illustrates a bistatic configuration that allows the use of a continuous-wave (or a very-high-repetition-rate) laser for generating synthetic beacons in the mesospheric sodium layer. In this approach, the outgoing beacon laser beam and the receiver aperture are separated. The separation must be large enough so that the receiver does not collect significant Rayleigh backscatter from lower altitudes. Conversely, if the separation is too large the beacon spot seen by the receiver has a highly elliptical shape. The ellipticity can degrade the performance of the wavefront sensor in the adaptive optics system. To date this approach has been rarely used.

The sodium layer lies at an altitude of approximately 90 km; the layer thickness is generally between 10 and 15 km. Laser radar studies of the sodium layer have been made for many years by research groups in several countries [9]. The abundance of sodium atoms (the number of atoms projected within a unit cross-sectional area of a vertical column extending over the layer thickness) varies with latitude, time of day, and season. An average value of the sodium abundance, as measured during our experiments in New Mexico (see next section), is approximately 3×10^{13} atoms/m^2. Although this average number of sodium atoms appears large, the number of nitrogen and oxygen molecules in the same column is many

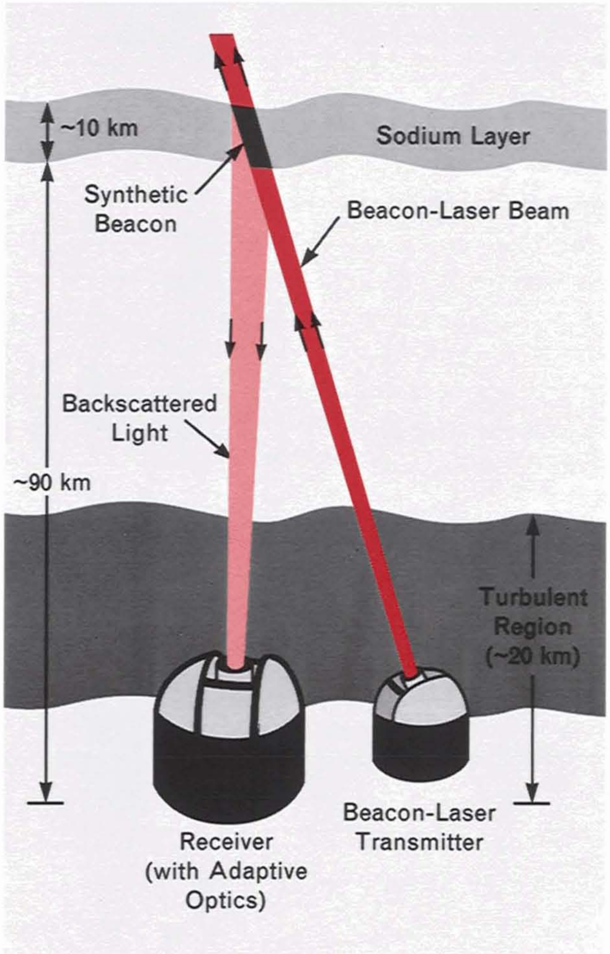

FIGURE 3. The bistatic approach to sodium-layer synthetic beacons. This configuration allows the use of a continuous-wave beacon laser, but only when generating synthetic beacons in the sodium layer. The separation between the beacon-laser transmitter and the receiver is such that only the illuminated sodium layer (and a small altitude region to either side of the layer) falls within the field of view of the receiver.

orders of magnitude higher. As this article will show, the synthetic-beacon laser must be carefully designed to make efficient use of the sodium atoms. The large differential cross section for resonance scattering of the sodium atom partially compensates for the low density.

To produce a useful synthetic beacon in the sodium layer, the laser must meet several requirements. Most importantly, the laser should have a narrow spectral bandwidth (3 GHz or less) and should be accurately tuned to the wavelength of a sodium line (usually the D_2 line at 589 nm) to produce resonant backscatter. Other requirements relate to the peak power, the spectral structure, and the pulse format of the laser. We discuss these requirements in more detail later in this article.

The performance that can be achieved by synthetic-beacon systems depends on several factors in addition to the laser source. These factors, which can affect measurement error, include focal anisoplanatism, beacon wavefront curvature, and beacon spot size. Furthermore, a suitable means must be provided for tracking the object of interest, because the synthetic beacon does not give information about the position of the object.

Focal Anisoplanatism

For synthetic-beacon applications such as astronomy or satellite imaging, the synthetic beacon is at a much closer range than the object of interest. Figure 4 illustrates how the light from the synthetic beacon does not traverse exactly the same path through the atmosphere as the light from an ideal conventional beacon located adjacent to the object. Note that for a low-altitude Rayleigh beacon, the turbulent region above the beacon is not sampled at all. The failure of the light from the synthetic beacon to pass through the desired atmospheric path introduces a wavefront error known as *focal anisoplanatism.* From the geometry illustrated in Figure 4 we can deduce that, for a fixed aperture size, the effect of focal anisoplanatism is less for a sodium-layer beacon than for a Rayleigh-backscatter beacon. Figure 5 shows the results of a theoretical calculation that supports this deduction. Supporting experimental data are offered later in this article.

Beacon Wavefront Curvature

A beacon source at a finite range contributes a curvature to the wavefront; if not taken into account, this curvature is another source of measurement error. For low-altitude beacons used with adaptive optics systems operating in the visible spectral region, the wavefront curvature must be accurately determined. Our calculations show, for example, that the curvature must be determined to an accuracy of approximately 50 m to introduce less than $\lambda/20$ error

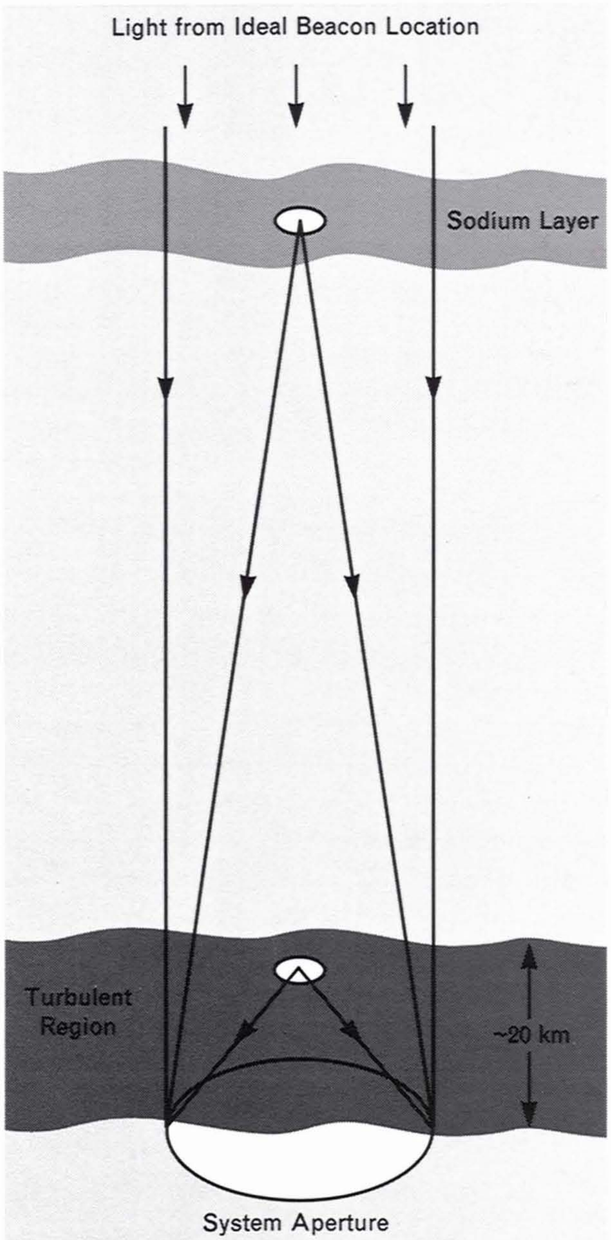

FIGURE 4. The different light paths through the atmosphere for light from an ideal distant beacon, a synthetic beacon in the sodium layer, and a low-altitude synthetic beacon produced by Rayleigh backscatter. For the conditions illustrated, the failure of the synthetic-beacon light to traverse the correct path results in a wavefront phase error known as focal anisoplanatism.

(λ = 0.5 μm) for a beacon range of 5 km and a receiving aperture with a diameter of 60 cm. Furthermore, a synthetic beacon can be regarded as a series of sources distributed axially and transversely, with the axial distance (altitude range) greatly exceeding the transverse size. For the sum of the phases from these sources at different positions, only one curvature can be removed. This restriction leads to two possible errors, one due to the transverse spreading and one due to the axial spreading. For a fixed aperture size, these errors decrease as the beacon altitude is increased. Thus the sodium beacon offers another advantage over low-altitude Rayleigh beacons.

Beacon Spot Size

In general, to provide good sensor performance the beacon spot size should be close to the diffraction limit of the wavefront-sensor subaperture. For sodium-layer beacons, this criterion may conflict with the need for a larger spot to avoid saturation effects in the sodium layer (saturation effects are discussed later in the article). Our analysis indicates, however, that the residual focal-anisoplanatism error, averaged over the full aperture, appears relatively unaffected by the size of the beacon spot. To support and explain this conclusion, Figure 6 shows a computer simulation of the phase errors from a point source and from a distributed source. Close inspection of the two figures reveals that a point source produces a smaller error

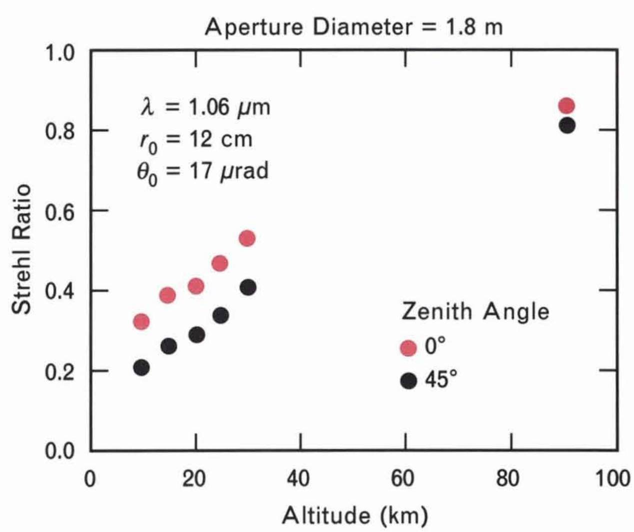

FIGURE 5. The effect of focal anisoplanatism on the Strehl ratio for beacons at several altitudes. This figure illustrates the advantage of using a sodium-layer (90-km) beacon over low-altitude Rayleigh-backscatter beacons. Calculations were not performed for altitudes between 30 and 90 km because the beacon-laser energies are usually excessive in this region.

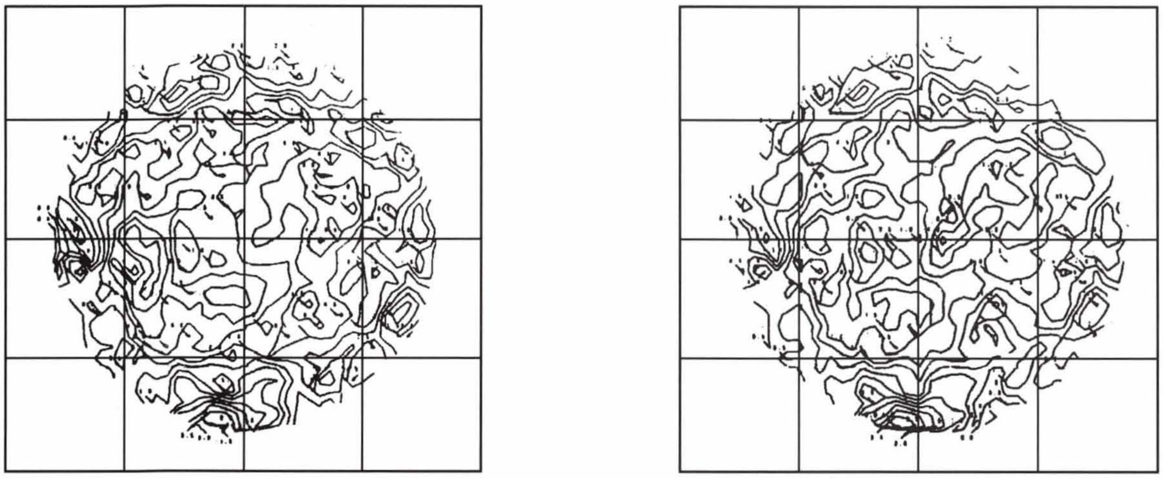

(a) (b)

FIGURE 6. Computer simulations showing the residual error of focal anisoplanatism over a receiver aperture for (a) a point source and (b) a distributed source. Both sources are at an altitude of 10 km. The receiver and the distributed source are 60 cm in diameter. Each contour plot is the difference between the plane-wave phase and the phase from the beacon; the contour lines of equal error are separated by 0.5 radian.

than the distributed source in the center of the aperture but a larger error at the edge. As a result, the focal-anisoplanatism error is relatively independent of source size, even for sizes approaching that of the receiver aperture.

Figures 7 and 8 illustrate how characteristics of the beacon spot depend on the projection approach. Both figures show computer simulations of the intensity distribution of a beacon-laser beam propagated through a turbulent atmosphere to the sodium layer at 90 km. In Figure 7 the laser beam was propagated through a 10-cm-diameter aperture without any correction for atmospheric turbulence. Our simulations showed changes in the shape and intensity distribution of the spot from pulse to pulse. These changes have a small effect on system performance when the spot is viewed by a computer-simulated adaptive optics system with a 3.5-m-diameter receiving aperture. In Figure 8 the beacon-laser beam is projected through the adaptive optics and out of the 3.5-m aperture; i.e., the beam is corrected for atmospheric turbulence. The spot in Figure 8, which was defocused to avoid saturating the sodium layer, is symmetrical but has a highly speckled appearance. Despite the different appearances of the two spots, our simulations showed that the turbulence-corrected spot improves the Strehl ratio of the system by an average of only 8% over the small uncorrected beam.

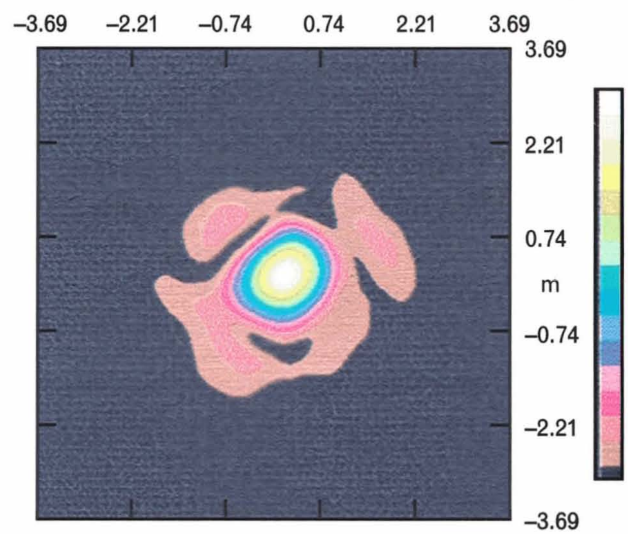

FIGURE 7. Computer simulation of a beacon spot in the sodium layer as formed by a laser beam propagated vertically through atmospheric turbulence from a 10-cm-diameter aperture. In this simulation the sodium layer was treated as a single plane. The color steps represent equal increments in the beam amplitude, i.e., the square root of the intensity.

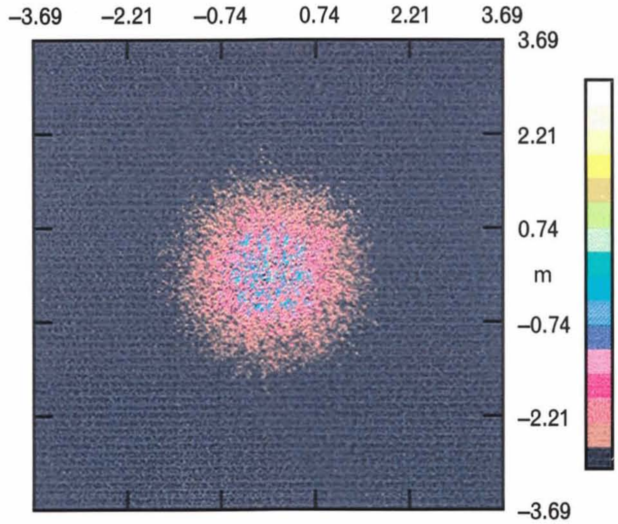

FIGURE 8. Computer simulation of a beacon spot in the sodium layer with the beacon-laser beam compensated for atmospheric turbulence. The beam was transmitted through a 3.5-m-diameter aperture and defocused so that much of the energy fell within a 1-m-diameter circle. Defocusing was needed to avoid saturation effects. The adaptive optics correction was based on turbulence information obtained from the previous laser pulse. The size of the speckles in the pattern is consistent with the diffraction limit of the transmitting aperture.

The Need for Independent Tracking

As was mentioned earlier, a synthetic beacon is not usable as a source of tracking information. The beacon-laser light makes both an upward and downward pass through the atmosphere. In doing so, overall tilt information is lost. Thus for tracking we require a sufficiently bright source close to the synthetic beacon (i.e., within the isoplanatic angle for tilt). The isoplanatic angle for tilt is typically a few times larger than the isoplanatic angle θ_0 [8]. Clearly, for visible and near-infrared wavelengths where θ_0 is typically 25 μrad or less, the likelihood of finding a bright tilt reference star near the object of interest is discouragingly small. Another approach to tilt tracking is needed; the lack of a suitable approach is a major concern in adaptive optics today.

Atmospheric-Turbulence Measurements with Synthetic Beacons

In late 1984 and early 1985, we made what are believed to be the first measurements of turbulence-degraded wavefronts with synthetic beacons in the sodium layer. These measurements were made at White Sands Missile Range (WSMR) in New Mexico. Figure 9 is a photograph of the WSMR facility used for the experiment. Measurements were also made on synthetic beacons generated by Rayleigh backscatter at altitudes from 6 to 20 km. The primary objective of the measurements was to demonstrate the feasibility of using resonant backscatter from the sodium layer as a synthetic beacon for wavefront compensation purposes. A secondary objective was to verify predictions that focal anisoplanatism was lower for a high-altitude sodium beacon than for low-altitude Rayleigh beacons. Our approach was to compare measured wavefronts from a synthetic beacon with those obtained simultaneously from a reference star boresighted to the beacon. After allowing for the effects of noise and other measurement errors, we found that the synthetic-beacon wavefront measurements (with overall tilt removed) showed reasonable agreement with those from the reference star. Furthermore, we showed that the effect of focal anisoplanatism does decrease as the beacon altitude is increased.

Figure 10 shows a simplified schematic of the test configuration. A pulsed dye laser (to be described later) served as the source for the synthetic beacon. The beam from this laser, after expansion to approximately 20 × 20 cm, was directed into the atmosphere by using an optical system known as the auxiliary beam director. The auxiliary beam director, illustrated simply as a single mirror in Figure 10, provided a clear aperture with a 1-m diameter. The divergence of the outgoing laser beam was carefully controlled to provide a small spot within the altitude range of interest. The angle subtended by the beacon spot, as measured at the detectors of a receiver system, was approximately 13 μrad for typical turbulence conditions.

By using a tracker to control the pointing of the auxiliary beam director, we boresighted the synthetic beacon to a bright star that provided a reference wavefront. The average phase gradients, or x-axis and y-axis tilts, of the wavefronts from the star and synthetic beacon were measured by two receiver systems. For simplicity, the diagram in Figure 10 shows that

FIGURE 9. Facility at White Sands Missile Range used for the sodium-layer experiment. The large dome contains the 1-m-aperture auxiliary beam director, which can be seen through the opening. The smaller dome contains a device to measure the atmospheric coherence length r_0. Other meteorological equipment is mounted on a nearby tower.

these receiver systems consisted of single lenses, dichroic beam splitters, and quadrant detectors; the photograph in Figure 11 shows that the real receiver systems were more complicated. Functionally these receivers can be regarded as two subapertures of a Hartmann wavefront sensor [10]. Each receiver system had an entrance diameter of 15 cm. The selection of subaperture size was driven by the modest energy of the laser. In view of the moderate seeing conditions at WSMR, the size chosen is larger than one would prefer for a high-performance adaptive optics system operating in the visible. The effect of the larger subapertures was taken into account during analysis of the effects of atmospheric turbulence.

A center-to-center subaperture separation of 76 cm was used between the two receiver systems; this separation was close to the limit set by the clear aperture of the auxiliary beam director. Because focal anisoplanatism increases with system aperture size, such a large subaperture separation was desired to facilitate the measurement.

The simple lenses shown in Figure 10 represent telescopes with a focal length of 32 m. Quadrant detectors at the foci of the telescopes measured the centroid displacement of the far-field spots formed by the respective wavefronts; the wavefront tilt was found by dividing the spot displacement by the focal length of the telescopes. To ensure the long-term stability of the telescopes, metering rods made of Super Invar controlled the spacing between the primary and secondary mirrors of the telescopes, and the mirror mounts were also made of Super Invar. Super Invar has an extremely low coefficient of thermal expansion; its use greatly decreased the sensitivity of the optical components to misalignment resulting from temperature changes. Because good alignment stability was essential to the success of this experiment, the optical-bench environment was kept constant (within ±1°C). Dichroic beam splitters separated the star and synthetic-beacon wavefronts and directed them to

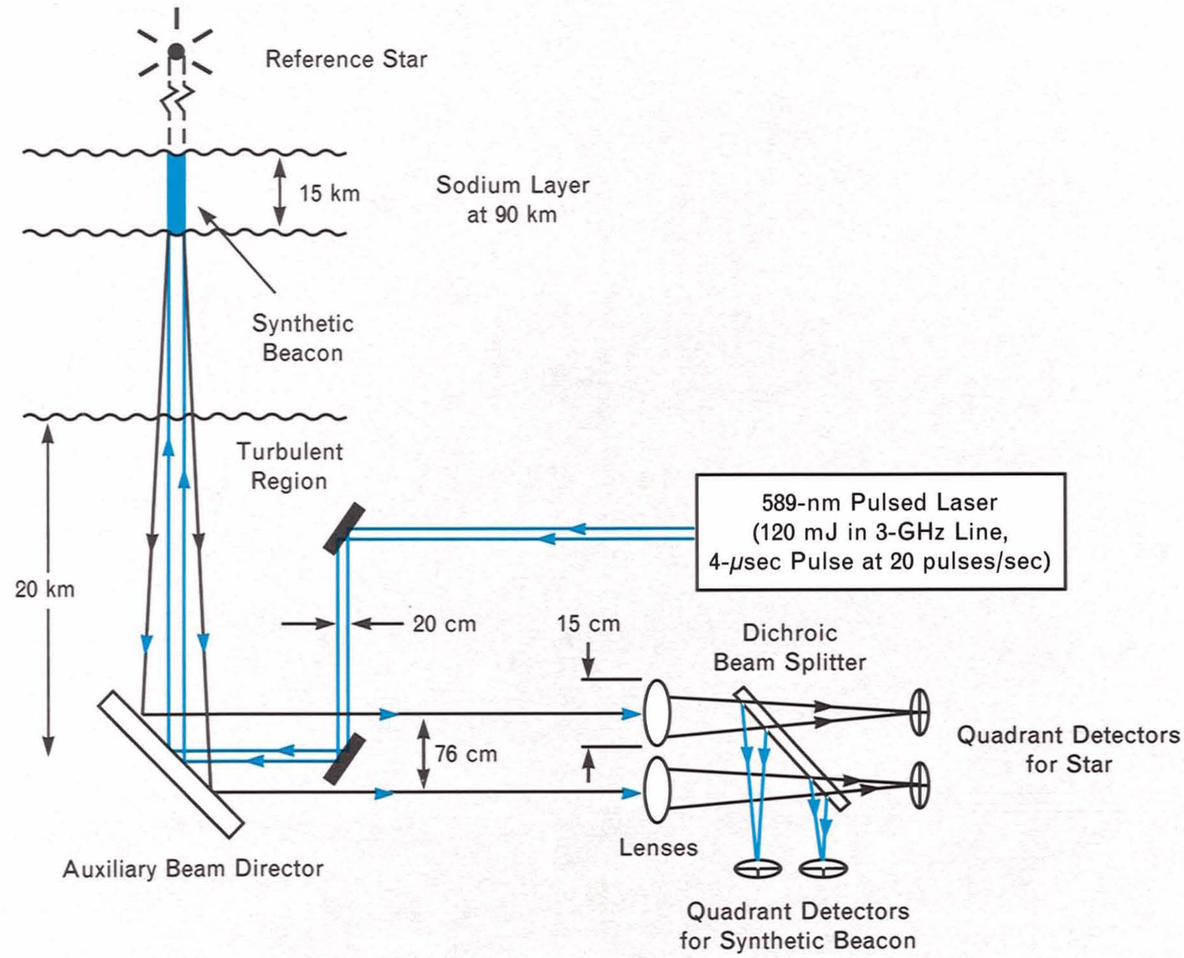

FIGURE 10. A diagram of the test configuration for atmospheric-turbulence measurements using a synthetic beacon in the mesospheric sodium layer. A pulsed-dye-laser beam was propagated to the sodium layer at an altitude of approximately 90 km. The backscatter from the laser spot served as a light source, or synthetic beacon. The synthetic beacon was boresighted to a bright star that provided a reference wavefront. Wavefront measurements were made on the beacon and star by using the two receiver systems that may be regarded as two subapertures of a Hartmann wavefront sensor.

their respective quadrant detectors. Narrow-bandpass spectral filters were used to minimize the leakage of stellar radiation onto the synthetic-beacon detectors.

Each far-field spot was focused at the apex of a four-sided pyramidal reflector. The pyramid sides reflected the light onto four photomultiplier tubes to provide a true quadrant detector. The low backscatter signals from the sodium beacons required photon-counting techniques. To reduce dark counts, cylindrical coils with circulating chilled water cooled the photomultiplier tubes to 12°C.

The photoelectrons from each photomultiplier tube were converted to serial pulse streams and summed in 16-bit counters; discriminators separated the photoelectrons from spurious signals. The start and summation times for these counters, relative to each laser pulse, were set from the main control panel, and provided the range gating needed to select the backscatter region. The numbers of detected photons for each integration period were fed into a NOVA 4X computer that recorded the counts from all photomultipliers and calculated tilt data for a real-time display. It also recorded calibration data for the quadrant detectors and timing information

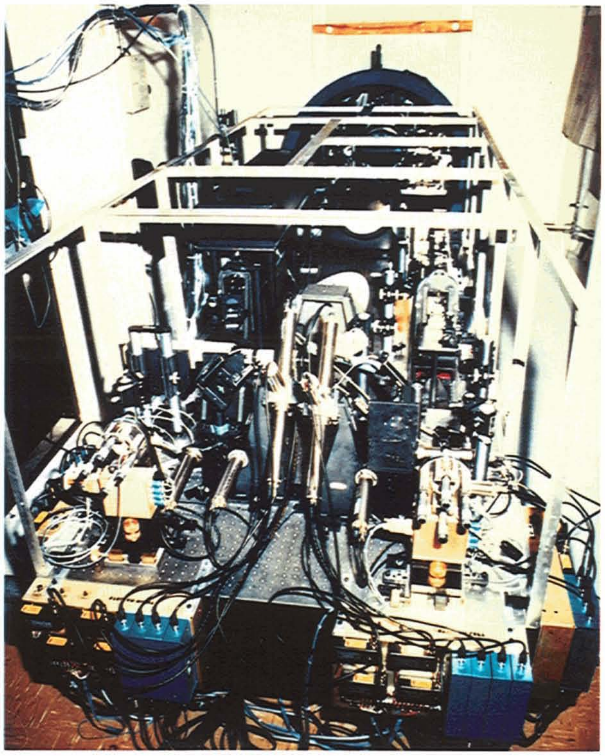

FIGURE 11. Optical bench with the transmitter and receiver telescopes. The cross-shaped assemblies in the foreground are the quadrant detectors. The arms of these assemblies house the photomultiplier tubes.

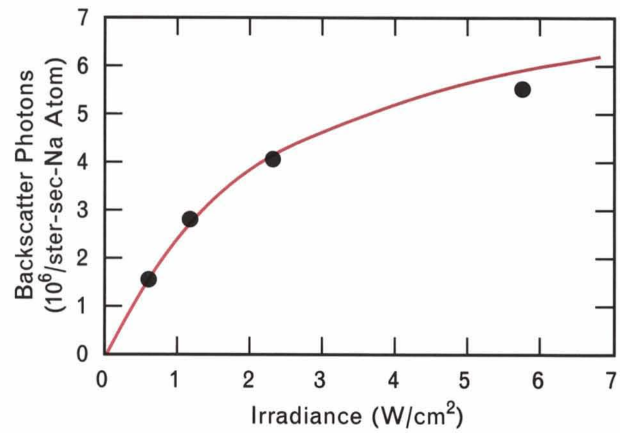

FIGURE 12. Theoretical calculations of sodium-layer backscatter as a function of the incident irradiance for the pulsed dye laser. The sodium atoms were assumed to be illuminated by circularly polarized laser light in the wavelength region of the D_2 resonance line at 589 nm. The modes of the laser were assumed to be uncorrelated. The atoms were segregated into 11 velocity groups and the weighted average of the backscatter from these groups was integrated over a thousand lifetimes (15.8 μsec). Because of saturation, there is little advantage in operating at irradiance levels in excess of 3 W/cm^2.

for the detector signals.

The need to provide a satisfactory return signal from the sodium layer without requiring significant technological advances dictated the choice of a laser for these experiments. At that time, in 1983, a flashlamp-pumped dye laser was determined to be the most suitable source. The laser requirements were based on detailed spectroscopic calculations of backscatter from the sodium layer; we discuss similar calculations later in this article.

From the spectroscopic calculations we determined that the spectral lineshape of the laser should be a smoothly varying function with a bandwidth of approximately 3 GHz (corresponding to 3.5 pm), tuned to the D_2 sodium line at a wavelength of 589 nm. This bandwidth was chosen to be larger than the optimum calculated width of approximately 2 GHz (1.5 times the Doppler width) to allow for frequency jitter or drift in the laser tuning. As a result of discussions with dye-laser manufacturers, we concluded that laser energies of up to 150 mJ within a 4-μsec pulse length could be expected. We also predicted that the area of the beacon cross section would be approximately 1.5 m^2, based on typical turbulence conditions anticipated at the site. By using these parameters and by taking into account the anticipated transmission losses, we predicted a peak irradiance of 2.5 W/cm^2 averaged over the beacon spot area. With this information and the results of our spectroscopic calculations (shown in Figure 12), we expected to detect approximately 100 photoelectrons for a 150-mJ pulse. These expectations proved optimistic, as the laser energy was lower than expected (see Table 1) and the optical-system transmission was also low. Keeping the

Table 1. Laser Characteristics

Wavelength:	589 nm
Bandwidth:	3 GHz
Typical Energy:	40 mJ/GHz
Beam Quality:	4 × diffraction limited
Pulse Length:	4 μsec
Pulse Repetition Rate:	20 pulses/sec

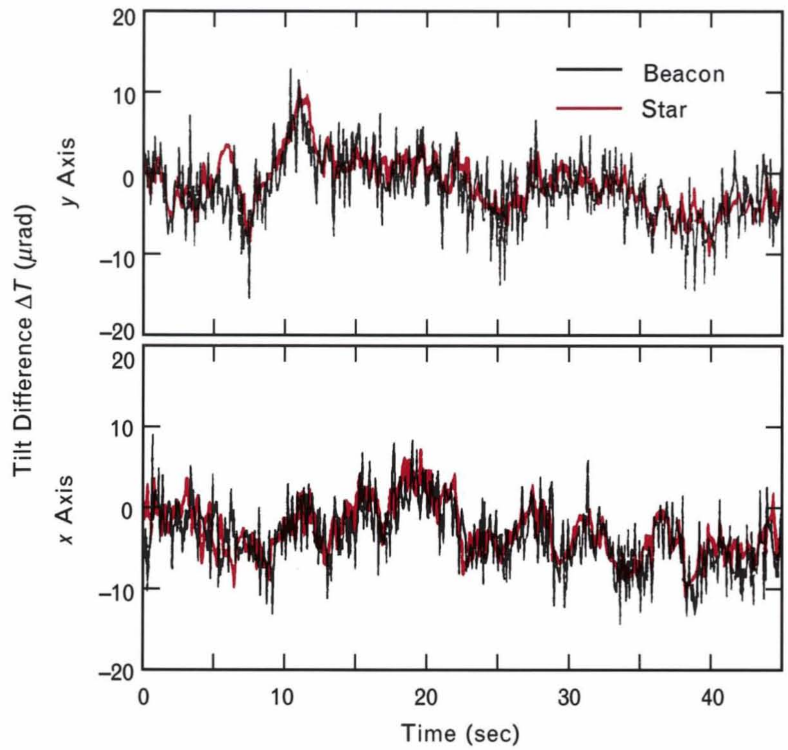

FIGURE 13. Comparison of the tilt differences for the star β-Gemini and a sodium-layer synthetic beacon. The low signals from the sodium layer result in a high level of photon noise for the synthetic-beacon signals. Aside from the differences in noise levels, the data for the synthetic beacon and β-Gemini are similar.

optics clean in the dusty desert environment was part of the problem. Our signals of a few tens of photoelectrons per pulse were still consistent with theory, assuming typical values for the sodium abundance. Much larger signals were, of course, obtained from the Rayleigh-backscatter beacons at low altitudes.

The pulsed dye laser was built and operated by Avco Everett Research Laboratory, which also provided diagnostics to monitor laser performance. The laser was configured as a master-oscillator power-amplifier chain. The oscillator and amplifier heads were originally built for an isotope separation program and were refurbished for our tests. Each laser head had two flashlamps that pumped Rhodamine 590 (6G) chloride dye. Four modulators linked to a command-charging circuit controlled the charging of the capacitors that provided energy to the flashlamps. The dc power supply of the laser could provide up to 15 kV at 20 A. Coarse wavelength selection was achieved with a diffraction grating installed in the optical train between the oscillator and amplifier. Fine tuning and bandwidth selection were performed by the insertion of etalons, also between the oscillator and amplifier.

The U.S. Army Atmospheric Sciences Laboratory at WSMR provided meteorological support for the experiment and data to correlate the test results with atmospheric conditions. In addition to standard measurements of temperature, humidity, and wind speed, they also measured turbulence parameters such as the atmospheric coherence length r_0 and the isoplanatic angle θ_0.

We performed our experiments at WSMR over a period of several months and made most measurements in the late evening. Turbulence conditions did not vary greatly except when the jet stream was positioned over WSMR. Average values of the coherence length r_0 were typically between 5 and 8 cm. Values of the isoplanatic angle θ_0 (not available for all tests) were usually between 7 and 10 μrad. As we expected, the high-altitude turbulence of the jet stream resulted in an increase in focal anisoplanatism. Measurements were made by using the sodium-layer beacon at 90 km as well as Rayleigh-backscatter beacons at altitudes in the range of 6 to 20 km. Bright stars such as Capella were used as reference sources.

Processing of the Tilt Data

We processed the tilt data from the reference star and the synthetic beacons to obtain a measure of focal anisoplanatism. This measure is defined by using variances of the tilt differences from the two receiver systems. We first consider the measured tilts from one pair of quadrant detectors, e.g., the detectors receiving starlight. These tilts, which are designated $T(1)$ and $T(2)$, can be separated into three components:

$$T(1) = T_O + T_H(1) + T_N(1)$$
$$T(2) = T_O + T_H(2) + T_N(2),$$

where T_O is the overall tilt, T_H is the higher-order contribution to tilt, and T_N is the tilt noise and other detector errors.

Overall tilt refers to any tilt component common to both receivers; for example, the quadrant detectors viewing the star see tracking jitter caused by the auxiliary beam director. We perform the following subtraction to remove overall tilt.

$$\begin{aligned}\Delta T &= T(1) - T(2) \\ &= T_H(1) - T_H(2) + T_N(1) - T_N(2).\end{aligned}$$

To compare the beacon and star tilt measurements, we then take the difference of the tilt differences to get

$$\delta T = \Delta T_{\text{beacon}} - \Delta T_{\text{star}}.$$

In processing the data, we determined the variance $\sigma_{\delta T}^2$ of δT. This variance was not zero for three reasons. First, focal anisoplanatism was present. A major objective of these measurements was, of course, to determine the magnitude of this effect. Second, the low backscatter signals resulted in significant photon noise, particularly for the sodium beacons. Third, errors were introduced by the quadrant detectors; e.g., the detectors are sensitive to variations in the spot sizes caused by atmospheric turbulence.

The variance $\sigma_{\delta T}^2$ of δT may thus be written in the following form:

$$\sigma_{\delta T}^2 = \sigma_{FA}^2 + 2\sigma_B^2 + 2\sigma_S^2 + \sigma_D^2, \qquad (1)$$

where σ_{FA}^2 is the variance of the focal-anisoplanatism term, σ_B^2 is the photon-noise contribution from one synthetic-beacon quadrant detector (the detector signals are assumed to be equal), σ_S^2 is the photon-noise contribution from one star quadrant detector, and σ_D^2 is the variance of other quadrant detector errors.

By rearranging Equation 1 we have

$$\sigma_{FA}^2 = \sigma_{\delta T}^2 - 2\sigma_B^2 - 2\sigma_S^2 - \sigma_D^2. \qquad (2)$$

In our experiment we determined the variances on the right side of Equation 2. An accurate determination of the photon-noise contribution was particularly important for the sodium-beacon measurements because here the photon-noise variance ($2\sigma_B^2$) usually exceeded the focal-anisoplanatism variance (σ_{FA}^2) by an order of magnitude. For the Rayleigh-beacon measurements, the situation was less stressing in that the photon noise was lower and the focal anisoplanatism was higher. Fortunately, our detector calibrations yielded excellent agreement with the predicted values of the photon-noise variance. We were therefore able to remove the photon-noise contribution with confidence. The focal-anisoplanatism variance (σ_{FA}^2) was determined by Equation 2. The measured values of σ_{FA}^2 were compared to theoretical calculations based on a turbulence model that represented conditions measured at the site.

In performing the theoretical calculations of σ_{FA}^2, we were able to show that the statistical properties of the average gradient, or tilt, over each receiver aperture can be approximated by a phase difference between two phase points at the edges of the aperture. This approximation resulted in a considerable simplification for the calculation of the angle-of-arrival statistics.

Figure 13 shows representative two-axis tilt-difference data (ΔT) for a sodium-layer beacon and the star β-Gemini. The x-axis of this figure refers to tilts measured parallel to the line joining the centers of the receiver apertures; the y-axis refers to tilts perpendicular to this line. The tilt differences measured with the beacon fluctuate considerably because of the high photon noise. Despite this noise, however, there is

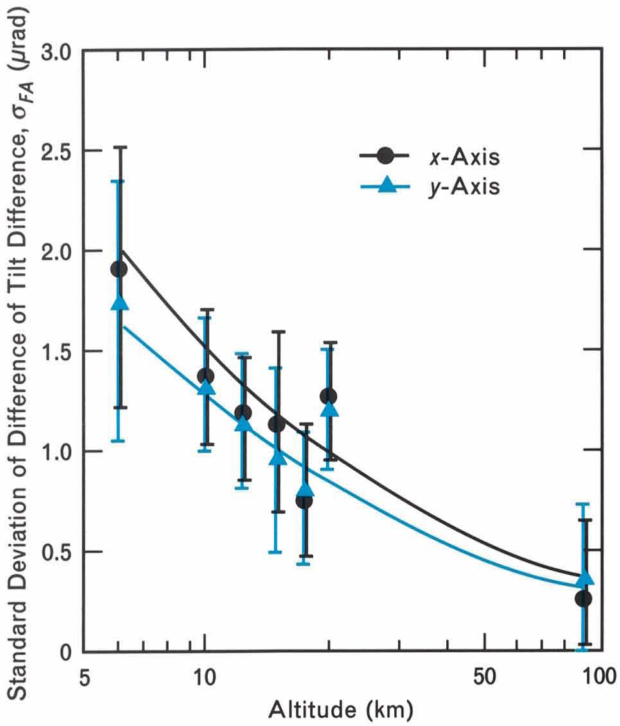

FIGURE 14. Summary of results for synthetic beacons generated by resonant backscatter in the sodium layer and lower-altitude Rayleigh backscatter. The black and red curves show the results of our theoretical predictions. Both the theoretical and experimental results exhibit a decrease in focal anisoplanatism as the beacon altitude increases.

generally good agreement between the tilt differences measured with the beacon and those measured with the star. This agreement indicates that we have actually made a phase measurement with a sodium-layer beacon. Although our tilt data are given in microradians, we can readily convert to wavelengths per subaperture; for example, 1 μrad is equivalent to 0.25 wavelength per subaperture, where λ is the laser wavelength of 589 nm. This conversion serves as a reminder that we are measuring phase gradients.

Figure 14 summarizes our results for both the sodium-layer beacons and the Rayleigh beacons at several altitudes in the range of 6 to 20 km. This figure shows the standard deviation of the focal-anisoplanatism term σ_{FA} as a function of beacon altitude. The black and red curves indicate the results of our theoretical predictions. We see that generally good agreement exists between theory and experiment, even though our turbulence model did not necessarily represent the turbulence conditions at our site. As expected, we observed a decrease in focal anisoplanatism as the beacon altitude increased. This experiment is believed to be the first experimental verification of the predicted behavior of a synthetic beacon in the mesospheric sodium layer. Furthermore, we provided the first demonstration that focal anisoplanatism is smaller for a sodium-layer beacon than for a lower-altitude Rayleigh beacon. These encouraging results prompted further experiments with synthetic beacons, as described in the article by Byron Zollars in this issue [11].

Synthetic-Beacon Technology

Earlier we alluded to some of the general requirements necessary for producing a useful synthetic beacon. This section provides further information on the beacon requirements and briefly describes the advanced sodium-layer beacon lasers under study at Lincoln Laboratory. We emphasize the sodium-layer beacon because, for a fixed aperture size, it offers the advantage of lower focal anisoplanatism than a low-altitude Rayleigh beacon. First, however, we review the positive aspects of Rayleigh beacons, as our intent is not to dissuade the reader from recognizing their utility.

Saturation effects that occur in the sodium layer are not a problem for Rayleigh scattering. For Rayleigh

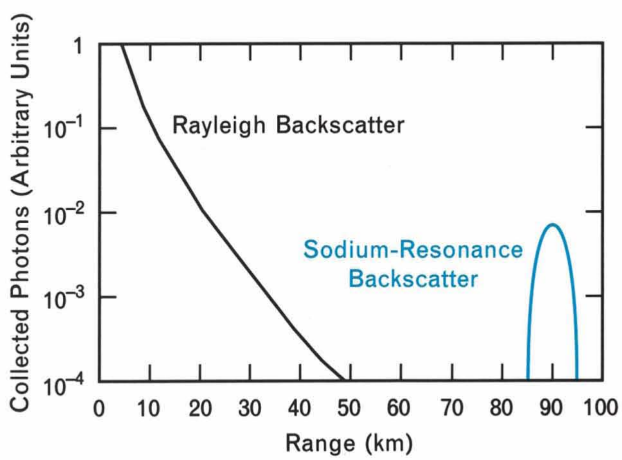

FIGURE 15. Relative backscattered photons at a receiver as a function of altitude for constant laser energy. The laser is appropriately tuned to 589 nm for resonant backscatter from the sodium layer. At altitudes of 10 km or less, the Rayleigh backscatter greatly exceeds the sodium-layer backscatter; thus lower laser powers are needed to generate low-altitude Rayleigh beacons.

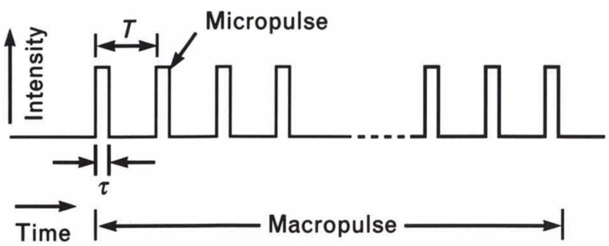

FIGURE 16. A section of a pulse train, or macropulse. The individual micropulses are identical, with a repetition time T. In our analysis, the value of T is 10 nsec (compared to a spontaneous decay lifetime of 16 nsec) and a macropulse contains on the order of 10^4 micropulses. The micropulse duration τ is a significant parameter in the performance of the laser system.

beacons we are not constrained to building a laser that has a narrow spectral bandwidth and requires accurate tuning to a resonant wavelength. Furthermore, the temporal structure (if any) of the laser output is unlikely to be important for Rayleigh beacons; we will see shortly that temporal structure is important for some sodium-layer beacon lasers.

At altitudes below 15 km we can obtain much higher backscatter signals from a Rayleigh beacon than from a sodium-layer beacon for a given laser-pulse energy, as illustrated in Figure 15. The data presented in this figure are for a wavelength of 589 nm. With Rayleigh beacons, however, we have freedom to select the wavelength; this freedom is, of course, constrained by the spectral transmission of the atmosphere and the quantum efficiency of available detectors. For Rayleigh backscatter, the number of received photons is inversely proportional to λ^3. (The $1/\lambda^4$ scaling typically associated with Rayleigh backscatter applies only to the scattered energy; in converting to photons we lose a factor of $1/\lambda$.)

The choice of synthetic-beacon type depends on other factors, including the system performance requirements, cost, schedule, and technical risk. Discussion of these factors is beyond the scope of this article.

Sodium-Layer Beacon

The challenge presented by the sodium layer is simple to describe—not many sodium atoms are up there. In addition, even at the most favorable laser frequency only about one photon in sixteen interacts with a sodium atom on its way through the layer. So we must take care to use the available atoms as effectively as possible. We shall see that this limitation leads to the development of a laser with carefully defined characteristics.

The first requirement is that the light be approximately resonant with the strongest sodium line, which is the well-known yellow D_2 line ($3^2S_{1/2} - 3^2P_{3/2}$) at a wavelength of 589 nm. At this wavelength two candidates for the narrowband beacon laser are a solid-state sum-frequency mode-locked laser and a free-electron laser (FEL), both of which deliver their energy in the form of trains of short pulses (500 psec for the mode-locked laser, 50 psec for the FEL).

The pulse trains should not last too long, so that the returns from the sodium layer do not overlap with those from the Rayleigh layer. This requirement determines a maximum length for a single pulse train of 100 to 200 μsec. Thus we are led to the concept of a laser that delivers long trains, or *macropulses*, of individual short pulses, or *micropulses*, as shown in Figure 16. We proceed to ask how a sodium atom will interact with the light from such a laser, and what characteristics of the pulses (pulse length and strength, time between pulses, central frequency of pulses, phase modulation) give rise to the greatest backscatter for a given amount of laser power.

We begin with a simplified model of a sodium atom in which only two energy levels are considered (the *two-level atom*), and study how such an atom interacts with a pulse train [12]. This simplification is not as extreme as it seems. We shall see that under the action of optical pumping the sodium atom essentially evolves to just this state. The basic facts about the response of a two-level atom to a single laser pulse are well known. For a pulse short enough that spontaneous decay can be ignored during the pulse, the response depends on two quantities: the pulse area

$$A_P \equiv \frac{1}{\hbar}\int pE(t)\,dt\,,$$

where p is the transition dipole moment and $E(t)$ the envelope of the electric-field pulse, and the detuning $\omega - \omega_0$ of the carrier wave from the resonant frequency, where the detuning is the difference between resonant and carrier frequencies. On resonance the system is a periodic function of A_P. When A_P equals π, an atom initially in the ground state is flipped up to the excited state, and vice versa, while when A_P equals 2π the atom is flipped from its original state to the other state and then back again. The response is thus not a monotonic function of the energy in the pulse, which is proportional to A_P^2/τ, where τ is the pulse length. Off resonance the response is smaller; the atom cannot be flipped completely by a single pulse. Furthermore, the relative phase between upper and lower states oscillates at a frequency equal to the difference between resonant and carrier frequencies (the detuning).

After a pulse passes, the atom begins to decay by the process of spontaneous emission (collisions between atoms are not important at the altitude of the mesosphere). But if another pulse arrives before the decay is completed, the response of the atom to the second pulse depends on the relative phase between upper and lower states: if the relative phase has changed by an integral multiple of 2π, then the effect of the first pulse (even a small one) is reinforced, so that during a long pulse train the mean fraction of the time spent in the excited state can be high (though never greater than one half). Thus in a gas of atoms at

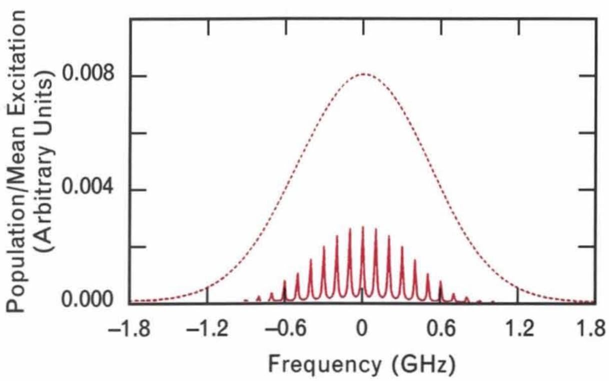

FIGURE 17. The dotted line shows the distribution of radial velocities of sodium atoms in the mesosphere (measured in units of the Doppler shift at the frequency of the D_2 line). The solid line shows the degree of excitation of these atoms (i.e., the fraction of time spent in the excited state) when a pulse train is incident upon it. The incident micropulses in this case have a pulse area $A_P = 0.2\pi$ and the pulse-repetition frequency is 100 MHz.

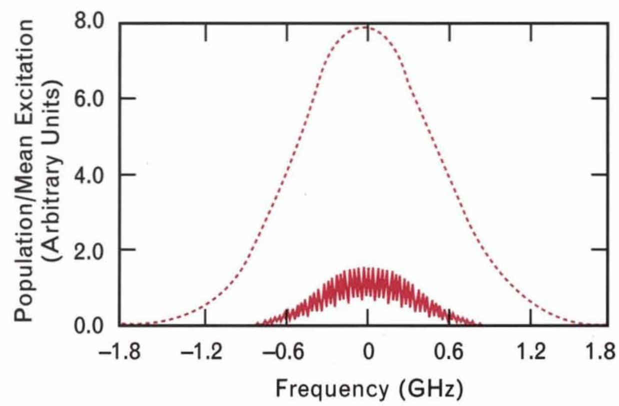

FIGURE 18. The same situation as in Figure 17, but the pulse train is now given a phase modulation of amplitude 0.75π and frequency 30 MHz. In this case considerably less variation occurs from peak to valley, and the overall efficiency of excitation is improved.

finite temperature, where the resonant frequencies are shifted by the Doppler effect, the mean excitation of the atoms shows peaks and valleys according to the radial velocities of the individual atoms. Figure 17 illustrates this variation of mean excitation with frequency.

Figure 17 clearly shows that while some of the atoms are being effectively excited, and therefore radiating strongly back to the receiver, most of them are not. To increase the overall efficiency for reradiating, we must interfere with the resonance associated with the interpulse time. Changing the relative phase of successive pulses achieves this interference. If the frequency of the phase modulation is such that the repeat time for the phase of a pulse is much longer than the spontaneous decay time, then the resonance effect is reduced and the mean excitation efficiency is improved. Figure 18 illustrates an example of the effect of phase modulation on the mean excitation.

Smoothing out the peaks of mean excitation has another, more subtle, effect. When an atom interacts with a beam of photons, each interaction on average imparts to the atom a momentum of $\hbar\omega/c$ in the direction of the photon beam. This momentum, though small, can change the velocity of the atom sufficiently in a region where collisions are infrequent so that atoms that were originally resonant with a sharp peak in the excitation function move into another velocity group, out of resonance. The velocity groups for which the backscatter is largest are most affected, and the total backscatter thus declines severely. Therefore, when the peaks are less pronounced, as they are in the phase-modulation regime, the decrease of the backscatter is considerably less severe. Figures 19 and 20 illustrate these effects without and with phase modulation.

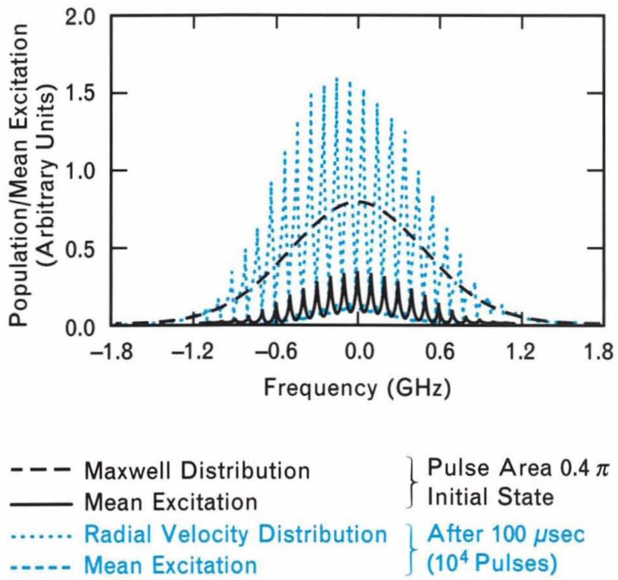

FIGURE 19. The effect of transfer of momentum from the photon stream to two-level atoms (the *light pressure*) in the absence of phase modulation. The sharp peaks of the initial excitation cause large oscillations in the radial velocity distribution after 10^4 pulses, with deep holes in the velocity distribution at the position of the original excitation peaks. The small peaks remaining in the excitation occur because of inefficient excitation at the peaks of the velocity distribution. In addition, the velocity distribution has an overall red shift.

With the real sodium atom, rather than the two-level model, the picture is considerably more complicated [13, 14]. Figure 21 illustrates the 16 sublevels in the upper state and the 8 sublevels in the lower state. The energy differences among the upper states are small, but the energy difference in the lower state between the sublevels labelled F = 2 and those labelled F = 1 is significant. This hyperfine structure results in the double-peaked intensity distribution of light absorbed by an assembly of sodium atoms in thermal equilibrium in the mesosphere, as shown in Figure 22.

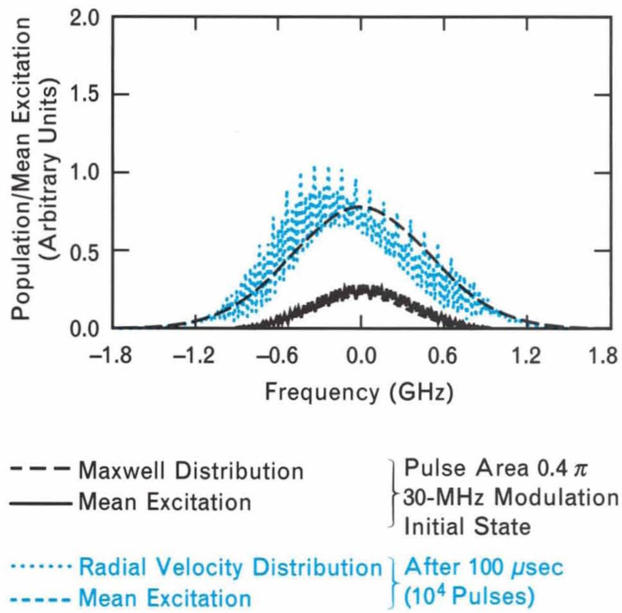

FIGURE 20. The effect of light pressure on two-level atoms in the presence of 30-MHz phase modulation. Compared with Figure 19, the oscillations in initial excitation and in final velocity distribution are less pronounced and the final excitation is smoother. The red shift is more pronounced because the overall excitation is more efficient.

When a sodium atom is illuminated by circularly polarized light, any of the transitions shown in Figure 21 between lower state sublevels and upper state sublevels are possible. Each transition imparts one

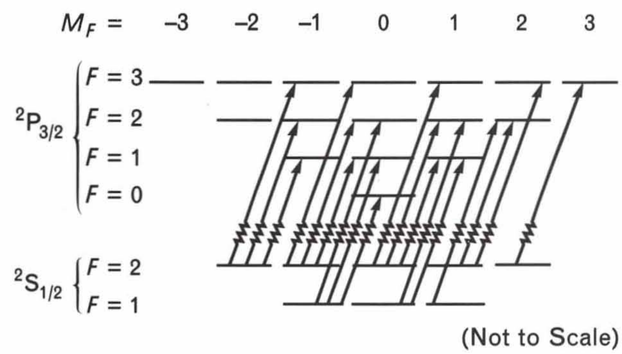

FIGURE 21. Energy-level diagram of the D_2 transition in sodium, showing the transitions allowed under illumination by right-circularly-polarized radiation. The quantum number M_F designates the number of units of angular momentum of the energy level projected along the z-axis (which is specified by the direction of the beam), while the quantum number F designates the total angular momentum. Each of the allowed transitions increases M_F by one unit.

unit of angular momentum to the atom. The atom then decays by spontaneous emission, which can cause it to give up one or zero units of angular momentum, or actually to add a unit. As a result then of repeated excitations followed by reemissions, the atom is gradually pumped from its initial state to a condition in which it oscillates between the two states of maximum angular momentum. This transition is precisely the one that interacts most strongly with the illuminating beam and reradiates most strongly backward in the direction that the illuminating beam is coming from. Thus the continued operation of optical pumping places the atom in a situation most favorable for backscatter; this situation is essentially that of the two-level atom discussed earlier.

We wish to design our pulse trains so that optical pumping is favored for all velocity groups, yet we need to to do this within the constraint of a given laser power output. The key to the problem is in the length of the individual micropulses and their central frequency. (We have already seen that phase modulation is needed to smooth out the responses from different velocity groups.) The micropulse length has two important effects: the shorter the micropulse, the wider the bandwidth of the radiation and the greater the energy required to achieve a given pulse area A_P, and thus a given excitation of the atoms. The bandwidth must be large enough so that it covers most of the hyperfine structure pattern shown in Figure 22, but any greater bandwidth is essentially thrown away. Detailed analysis shows that the optimum micropulse length is in the range 500 to 700 psec, corresponding to a bandwidth of 2.0 to 1.4 GHz. Although faster optical pumping is achieved when the central frequency is located near the centroid of the hyperfine structure pattern, that advantage is overweighed by the increased excitation efficiency achieved by locating the central frequency at the maximum of the pattern.

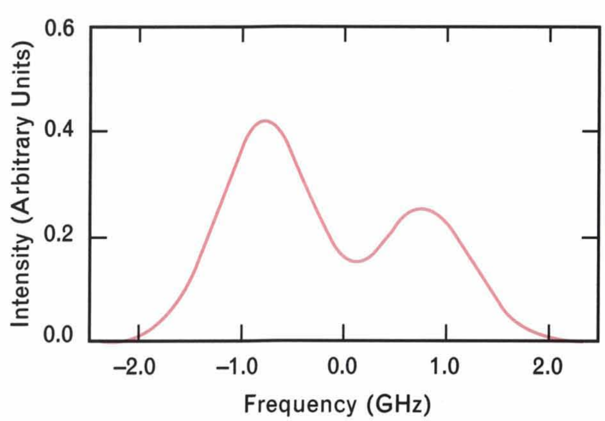

FIGURE 22. Doppler-broadened hyperfine structure of the sodium D_2 transition. The splitting is almost entirely due to the splitting in the $^2S_{1/2}$ ground state. The ratio of the areas under the two peaks—5:3—is equal to the ratio of the number of M_F levels characterized by the quantum numbers $F = 2$ and $F = 1$, respectively.

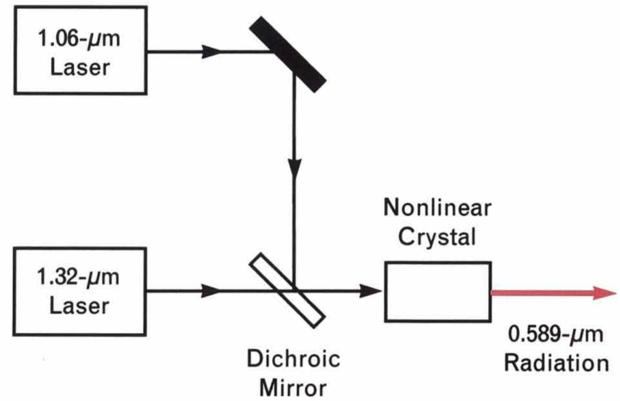

FIGURE 23. Sum-frequency generation of sodium-resonance radiation. The diagram show the generation of 589-nm radiation by sum-frequency-mixing the 1.06-μm and 1.32-μm outputs of two Nd:YAG lasers in a nonlinear crystal.

Development of Sodium-Layer Beacon Lasers

The sodium-layer experiment performed at WSMR used a pulsed dye laser. Although this laser sufficed for that experiment, higher performance lasers are obviously needed for use with adaptive optics systems. Thus our attentions turned to more advanced lasers that offer the potential to operate at higher powers and repetition rates with greater efficiency and reliability. Two lasers of particular interest are a solid-state sum-frequency laser and the FEL. Lincoln Laboratory has made considerable progress in developing the sum-frequency laser. The FEL has been the subject of a feasibility study performed by the MIT Plasma Fusion Center [15]. Both lasers are feasible for an adaptive optics system, but the technical risks and costs are greater for the FEL.

The FEL study examined the feasibility of building a laser with an energy of 7 J/pulse in 100-μsec macropulses at a 1-kHz repetition rate, thus providing an average power of 7 kW. Military requirements demanded this level of performance; such high powers are unlikely to be needed for most astronomical applications, and the FEL is not considered an attractive candidate for these applications. Other important specifications were a micropulse separation of 10 nsec and spectral bandwidth of 3 GHz or less. Several FEL design options were considered in the course of the MIT study, and a radio-frequency linac operating at 120 MeV was selected for detailed analysis. The FEL gain and efficiency were calculated by using a nonlinear model; the results indicated that the output power could be achieved from an FEL operating at above 1% efficiency with a conventional radio-frequency accelerator. Numerical studies of the spectral evolution of an optical FEL oscillator with a grating rhomb were also performed. The rhomb, which consists of a pair of optical diffraction gratings, is employed to suppress sideband instability. The analysis showed that a signal with a bandwidth of 2 GHz could be obtained. Although the results of the design study are considered encouraging, an FEL of this type would require a major development effort to build and involve high technical risk.

The sum-frequency laser is, however, now being used for sodium-layer measurements. More detailed information on the use of sum-frequency lasers can be found in an article by T.H. Jeys in a previous issue of this journal [16]. Figure 23 shows a greatly simplified schematic layout of the device. The concept, suggested by Aram Mooradian of Lincoln Laboratory [17], is based on a remarkable coincidence of nature. Sum-frequency-mixing the output of a 1.06-μm Nd:YAG laser with that of a 1.32-μm Nd:YAG laser can generate sodium-resonance radiation at a wavelength of 589 nm. The lasers are operated at wavelengths close to the peak of their tuning curves to obtain this radiation. Lithium iodate ($LiIO_3$) and lithium triborate (LiB_3O_5) have both been used for sum-frequency generation; average mixing efficiencies of 30% have been achieved with these materials. The relatively poor spatial and temporal overlap of the two laser beams currently limits efficiency. The sum-frequency lasers built to date have all used flashlamp pumping; the use of diode lasers for pumping should result in better mixing efficiencies at higher powers. This increased efficiency occurs for two reasons. First, diode lasers are more efficient and produce lower thermal loads on the Nd:YAG than flashlamps, which results in better beam quality at higher laser output powers. Second, we can exercise greater control over the temporal output of a diode laser, which improves the temporal characteristics of the laser beam.

Two flashlamp-pumped sum-frequency lasers have recently been completed at Lincoln Laboratory. One is a 0.5-J, 10-Hz device currently being used in sodium-layer measurements at Lincoln Laboratory. The other is a 24-mJ, 840-Hz laser built for the Air Force Phillips Laboratory. This laser is also intended for use in sodium-layer experiments. Furthermore, Lincoln Laboratory recently completed the design of a 200-W diode-laser-pumped sum-frequency laser. A laser of this power would be suitable for astronomical applications requiring high-quality compensated images in the visible spectral region.

Summary

Synthetic beacons can be used as sources for atmospheric-turbulence compensation when conventional beacon sources are unavailable or inappropriate. In astronomy, for example, synthetic beacons can be used when the object of interest lacks sufficient brightness for wavefront-sensor operation or a suitably bright object is not close by. The astronomer must still depend on a nearby tracking star for image stablization, however, as a synthetic beacon provides no information about tilt.

The beacons are generated by resonant backscatter of laser radiation in the sodium layer or by Rayleigh backscatter at lower altitudes. For a fixed aperture, a sodium-layer beacon exhibits significantly less focal anisoplanatism than a lower-altitude Rayleigh-backscatter beacon. The laser requirements for a sodium beacon are, however, more demanding than for a Rayleigh beacon. For efficient utilization of the sodium atoms, the laser must have a narrow linewidth and be accurately tuned to the resonant wavelength.

In 1985 we showed experimentally that synthetic beacons can be used to measure the effect of atmospheric turbulence on a wavefront. The success of the experiment prompted Lincoln Laboratory to carry out experiments using synthetic beacons with an adaptive optics system to provide good atmospheric-turbulence compensation. In addition, Lincoln Laboratory has been actively developing a sum-frequency solid state laser for generating a sodium-layer synthetic beacon.

Acknowledgments

The authors thank the many persons who participated in the experiment at WSMR. We regret that the number of participants is too large to acknowledge individually. Avco Everett Research Laboratory provided and operated the pulsed dye laser, and Dynalectron Corporation was responsible for many aspects of the operation of the auxiliary beam director. We gratefully acknowledge the support provided by several organizations at WSMR, including the Directed Energy Directorate, the National Range Operations Directorate, and the Atmospheric Sciences Laboratory.

We also thank Richard J. Temkin and his colleagues at the MIT Plasma Fusion Center for their valuable contributions to the FEL design study. We are grateful to Thomas H. Jeys for information provided on the sum-frequency laser and to Jonathan Schonfeld for his computer simulations of beacon spots in the sodium layer.

This work was supported by the Defense Advanced Research Projects Agency, the U.S. Army Strategic Defense Command, and the Department of the Air Force.

REFERENCES

1. R.E. Hufnagel, "Variations of Atmospheric Turbulence," *Digest of Technical Papers, Topical Meeting on Optical Propagation through Turbulence, Opt. Society of America, Washington, 9–11 July 1974.*
2. W. Happer and G. MacDonald, JASON Report JSR-82-106, MITRE Corp., McLean, VA (1983).
3. R. Foy and A. Labeyrie, "Feasibility of Adaptive Telescope with Laser Probe," *Astr. Astrophys.* **152,** 129 (1985).
4. R.Q. Fugate, D.L. Fried, G.A. Ameer, B.R. Boeke, S.L. Browne, P.H. Roberts, R.E. Ruane, G.A. Tyler, and L.M. Wopat, "Measurement of Atmospheric Wavefront Distortion Using Scattered Light from a Laser Guide Star," *Nature* **353,** 144 (1991).
5. R.A. Humphreys, C.A. Primmerman, L.C. Bradley, and J. Herrmann, "Atmospheric-Turbulence Measurements Using a Synthetic Beacon in the Mesospheric Sodium Layer," *Opt. Lett.* **16,** 1367 (1991).
6. L.A. Thompson and C.S. Gardner, "Experiments on Laser Guide Stars at Mauna Kea Observatory for Adaptive Imaging in Astronomy," *Nature* **328,** 229 (1987).
7. J.M. Beckers, P.J. Roddier, P.R. Eisenhardt, L.E. Goad, and K.-L. Shu, "National Optical Astronomy Observatories (NOAO) Infrared Adaptive Optics Program I: General Description," *Proc. SPIE* **628,** 290 (1986).
8. R.R. Parenti, "Adaptive Optics for Astronomy," in this issue.
9. E.D. Hinkley, ed., *Laser Monitoring of the Atmosphere* (Springer-Verlag, Berlin, 1976).
10. R.R. Parenti, "Recent Advances in Adaptive Optics Methods and Technology," *Proc. SPIE* **1000,** 101 (1988).
11. B.G. Zollars, "Atmospheric-Turbulence Compensation Experiments Using Synthetic Beacons," in this issue.
12. L.C. Bradley, "Atomic Excitation by a Pulse Train, Paper I: Two-Level Atoms," *Opt. Society of America Ann. Mtg., Boston, 4–9 Nov. 1990.*
13. L.C. Bradley, "Atomic Excitation by a Pulse Train, Paper II: Sodium," *Opt. Society of America Ann. Mtg., Boston, 4–9 Nov. 1990.*
14. L.C. Bradley, "Pulse-Train Excitation of Sodium for Use as a Synthetic Beacon," submitted to *J. Opt. Soc. Am. B.*
15. S.C. Chen, B.G. Danly, R.J. Temkin, J. Wurtele, and B. Yang, "Design Study of a 7-kW, Visible Wavelength FEL," Final Report for the year Sept. 1989–Aug. 1990, MIT Plasma Fusion Center.
16. T.H. Jeys, "Development of a Mesospheric Sodium Laser Beacon for Atmospheric Adaptive Optics," *Lincoln Laboratory J.* **4,** 133 (1991).
17. T.H. Jeys, A.A. Brailove, and A. Mooradian, "Sum Frequency Generation of Sodium Resonance Radiation," *Appl. Opt.* **28,** 2588 (1989).

RONALD A. HUMPHREYS
is assistant leader of the High-Energy-Laser Beam Control and Propagation group. His focus of research is in adaptive optics for high-energy laser beam control systems. He received his B.Sc. degree in physics from the University of Southampton, England, and he has been at Lincoln Laboratory for 14 years. Ron was the leader of the team that made the first measurements on sodium-layer synthetic beacons described in this article.

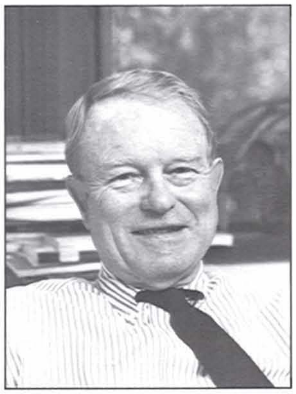

LEE C. BRADLEY
is a senior staff member in the High-Energy-Laser Beam Control and Propagation group. His research interest is in nonlinear optics, and he has been at Lincoln Laboratory for 26 years. Lee received a B.A. in physics from Princeton University and a Ph.D. degree in physics as a Rhodes Scholar at Oxford University.

JAN HERRMANN
is a staff member in the High-Energy-Laser Beam Control and Propagation group. His research speciality is in adaptive optics, and he has been at Lincoln Laboratory for 30 years. His undergraduate and graduate studies were at the University of Vienna, where he received a Ph.D. in physics.